Supporting Information

Ortiz et al. 10.1073/pnas.1401952111

SI Materials and Methods

Magnetic Resonance Imaging. Brains of injected mice were scanned at 8-, 11-, 16-, and 20-wk postinjection with a 200 MHz Bruker 4.7T Biospec MRI scanner equipped with a 560 mT/m ID 12-cm gradient (Bruker Biospin MRI; Resonance Research). For mouse brain imaging, brain coronal T2-weighted images using fast spin-echo RARE sequence (Rapid Acquisition with Relaxation Enhancement) was acquired with TR 1.5 s, TE 50 ms, RARE factor of 8, slice thickness of 0.7 mm, field of view 30 × 20mm, in-plane resolution of 117 × 125 μM, and 24 averages. Tumor volume was calculated by contouring, measuring the tumor areas, and calculating the sum of the areas multiplied by the distance between the centers of two adjacent slices.

Histology and Immunostaining. Brains from mice were collected and fixed with 10% (vol/vol) neutral buffered formalin (Sigma). Tissues were embedded in paraffin and 5-μm sections were used for analysis. Sections were stained with H&E or used for immunohistochemical analysis.

Immunohistochemistry was performed at the Molecular Cytology Core Facility of Memorial Sloan-Kettering Cancer Center using Discovery XT processor (Ventana Medical Systems). Tissue sections were stained with the following antibodies: p-Stat3 Tyr-705 (Cell Signaling, cat. no. 9145; rabbit monoclonal, 0.5 μg/mL), Stat3 (Cell Signaling, cat. no. 9132; rabbit polyclonal, 0.16 μg/mL), Iba1 (Wako Chemicals, cat. no. 019–19741; rabbit polyclonal, 0.5 μg/mL), Gfap (Dako, cat. no. Z033429-2; rabbit polyclonal, 1 μg/mL), Olig2 (Millipore, cat. no. AB9610; rabbit polyclonal, 2 μg/mL), and Nestin (BD Pharmigen, cat. no. 556309; mouse monoclonal, 5 μg/mL). For rabbit antibodies, tissue sections were blocked in 10% (vol/vol) goat serum with 2% (wt/vol) BSA in PBS. For the mouse antibody, tissues were blocked with Biotinylated Mouse on Mouse (M.O.M.) anti-Mouse Ig Reagent (Vector Labs, cat. no. MKB-2225). Primary antibody incubation was done for 5 h, followed by a 60-min incubation with biotinylated goat anti-rabbit IgG (Vector Labs, cat. no. PK6101; 1:200 dilution) or biotinylated anti-mouse IgG (Vector Labs, cat. no. BMK-2202) according to the manufacturer's instructions. Detection was performed with Blocker D, Streptavidin-HRP and DAB kit (Ventana Medical Systems) according to the manufacturer's instructions. Slides were counterstained with hematoxylin and cover-slipped with Permount (Fisher Scientific).

CD34 staining was performed on the Leica Bond RX (Leica Biosystems) using the Bond Polymer Refine Detection Kit (Leica Biosystems, DS980). Anti-CD34 antibody (Abcam, cat. no. ab8158; rat monoclonal, 16 μg/mL) was added for 30 min followed by a 30-min incubation of biotinylated anti-rat (Vector Labs, cat. no. BA-4001; 1:100 dilution). TUNEL staining was performed with the following reaction mixture: 0.1 M sodium cacodylate pH 7, 0.1 mM DTT, 0.05 mg/mL bovine serum albumin, 2 U/μl terminal transferase, 0.2 nm biotin-16-dUTP, and 2.5 mM cobalt chloride for 1 h at 37°. The reaction was terminated with 300 mM sodium chloride and 30 mM sodium citrate at room temperature for 15 min, incubated in avidin-biotin for 30 min, and developed with 3,3′-diaminobenzidine for 3 min.

Dual immunofluorescence of p-Stat3 and Iba1 or Gfap were performed using Discovery XT processor (Ventana Medical Systems). Staining with p-Stat3 Tyr-705 (Cell Signaling, cat. no. 9145; rabbit monoclonal, 0.5 μg/mL) followed by Tyramide Alexa Fluor 568 (Invitrogen, cat. no T20914) was performed first. Next, Iba1 (Wako Chemicals, cat. no. 019–19741; rabbit polyclonal, 0.5 μg/mL) or Gfap (BD Pharmigen, cat. no. 561483; mouse monoclonal, 5 μg/mL) was added followed by Tyramide-Alexa Fluor 488 (Invitrogen, cat. no. T20922).

Immunostaining Image Analysis. Whole slides were scanned with Pannoramic Flash Scanner (3DHistech). Image analysis of tumor areas was performed with Metamorph software (Molecular Devices). For analysis of immunohistochemistry images, color thresholds were set for brown positive staining and for total area (brown staining + blue nuclei). Percent of brown staining to total area was calculated. For analysis of dual immunofluorescence images, a grayscale threshold and standard area was set for green (Iba1), red (p-Stat3), and blue (DAPI). For each sample, the number of DAPI-positive nuclei within each stained area, and the number of DAPI within colocalized areas was calculated.

Human Tumor Collection, Tissue Lysates, and Immunoblotting. Fresh human glioblastoma multiforme (GBM) tissue samples were obtained from patients who consented under an Institutional Review Board-approved protocol. Tumor lysates were lysed in CelLytic MT Mammalian Tissue Lysis/Extraction Reagent (Sigma) supplemented with Complete Mini EDTA-free (Roche) and PhosSTOP (Roche) protease inhibitor mixes. Protein lysates were run in SDS/PAGE gels and transferred to nitrocellulose for immunoblotting. The following antibodies were used: p-STAT3 Tyr-705 (Cell Signaling, cat. no. 9145; rabbit monoclonal, 1:2,000) and STAT3 (Cell Signaling, cat. no. 9132; rabbit polyclonal, 1:1,000). Quantification of Western blot by densitometry analysis was performed using ImageJ software.

Flow Sorting of RCAS PDGF-GFP Tumors. Tumors were dissected from mice injected with replication-competent avian sarcoma-leukosis virus long terminal repeat with splice acceptor retrovirus (RCAS) PDGF-GFP and enzymatically and mechanically dissociated into single-cell suspensions by treatment with papain and ovomucoid as previously described (1). Single-cell suspensions were made in PBS with 10% (vol/vol) FBS, and GFP^+DAPI^- cells were sorted on a MoFlo Cell Sorter (Dako Cytomation).

Human Genetic Analysis and Microarray Analysis of Mouse Tumor Cells. The Cancer Genome Atlas data used was previously described (2, 3). The GBM oncoprint was generated using the cBio Portal as previously described (4)

Sorted GFP^+DAPI^- tumor cells from mice injected with RCAS-PDGF-GFP were stored at −80 °C in TRIzol LS Reagent (Ambion). Samples were processed by the Memorial Sloan-Kettering Cancer Center Genomics Core. Briefly, RNA was extracted and quality checked using a bioanalyzer. RNA was analyzed using the Affymetrix MOE 430A 2.0 chip following the manufacturer's instructions. Differentially expressed genes were determined using ANOVA. Principal component analysis and hierarchical analysis were performed using the Partek Software Suite. Genes were considered to be differentially expressed if their fold-change > 1.8 and P value < 0.05. Enriched pathways were identified using Ingenuity Pathway Analysis (Ingenuity Systems, Qiagen). Pathways with Benjami–Hochberg multiple testing correction P value < 0.05 and Bias-corrected z-score > 2 were considered to be significant.

Side Population Assay. Tumors were dissected from mice injected with RCAS PDGF-GFP and dissociated into single-cell suspensions, as previously described (1). Single-cell suspensions were made in unsupplemented basal neural stem cell media (Lonza) and counted using a hemocytometer. Side population

analysis was performed by Hoechst 33342 exclusion as previously described (5). Cells were incubated with or without verapamil (Sigma) and fumitremorgin c (Sigma) ABC inhibitors to set side population gates (5). Flow cytometry was performed with a MoFlo Cell Sorter (Dako Cytomation) and analysis was performed using Flojo software (Treestar Inc.).

***K_i*67 and GFP Flow Cytometry.** Tumors were dissected from mice injected with RCAS PDGF-GFP and dissociated into single-cell suspensions as previously described (1). Single-cell suspensions were made in PBS and counted using a hemocytometer. The following protocol was performed to minimize quenching of native GFP in the tumor cells. One million cells were fixed with 1% paraformaldehyde in a buffer made of HBSS and 2% (vol/vol) fetal bovine calf serum overnight at 4 °C. Cells were permeabilized using 0.5% TritonX-100 in HBSS and 2% (vol/vol) FBS for 10 min at room temperature. K_i67 antibody conjugated to Alexa 647 (BD Pharmigen, cat no. 561126; mouse monoclonal, 1/60 dilution) was made in HBSS:2% (vol/vol) FBS and applied to cells for 1 h at room temperature. Cells were washed two times with HBSS:2% (vol/vol) FBS and suspended in PBS:10% (vol/vol) FBS for analysis with a FACSCalibur (BD Biosciences). Analysis was performed using FloJo software (Treestar Inc.).

Flow Cytometry for Nestin. Single-cell suspensions of neonatal mouse days 1–3 brains were made using papain digestion as done previously. Staining was performed as described previously using Nestin antibody (BD Pharmigen, mouse monoclonal, cat. no. 556309; 1.7 μg/mL) and goat anti-mouse Alexa 568 (Life Technologies, cat. no. A21124; 33 μg/mL) (1). Flow cytometry was performed on the FACSCalibur (BD Biosciences), and analysis was performed using FloJo software (Treestar Inc.).

Statistical Analysis. Unless noted, Student *t* test was performed for all statistical analysis. Log-rank statistical analysis was performed for Kaplan–Meier curves and Fisher's exact test was performed for the tumor grade analysis.

1. Ciznadija D, Liu Y, Pyonteck SM, Holland EC, Koff A (2011) Cyclin D1 and cdk4 mediate development of neurologically destructive oligodendroglioma. *Cancer Res* 71(19): 6174–6183.
2. Cancer Genome Atlas Research Network (2008) Comprehensive genomic characterization defines human glioblastoma genes and core pathways. *Nature* 455(7216):1061–1068.
3. Verhaak RG, et al.; Cancer Genome Atlas Research Network (2010) Integrated genomic analysis identifies clinically relevant subtypes of glioblastoma characterized by abnormalities in PDGFRA, IDH1, EGFR, and NF1. *Cancer Cell* 17(1):98–110.
4. Cerami E, et al. (2012) The cBio cancer genomics portal: an open platform for exploring multidimensional cancer genomics data. *Cancer Discov* 2(5):401–404.
5. Bleau AM, et al. (2009) PTEN/PI3K/Akt pathway regulates the side population phenotype and ABCG2 activity in glioma tumor stem-like cells. *Cell Stem Cell* 4(3):226–235.

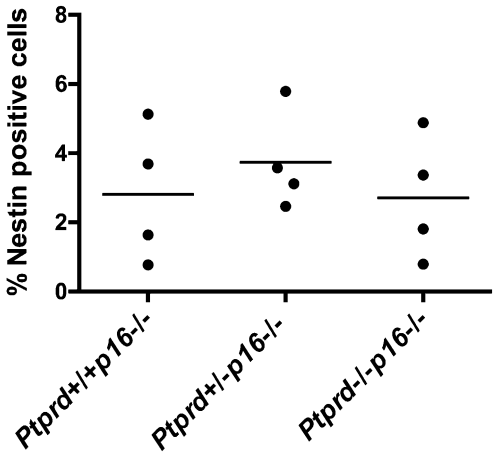

Fig. S1. Protein tyrosine phosphatase receptor-δ (*Ptprd*) loss does not affect frequency of Nestin$^+$ cells. Nestin flow cytometry of neonatal uninjected mice. Bars represent means.

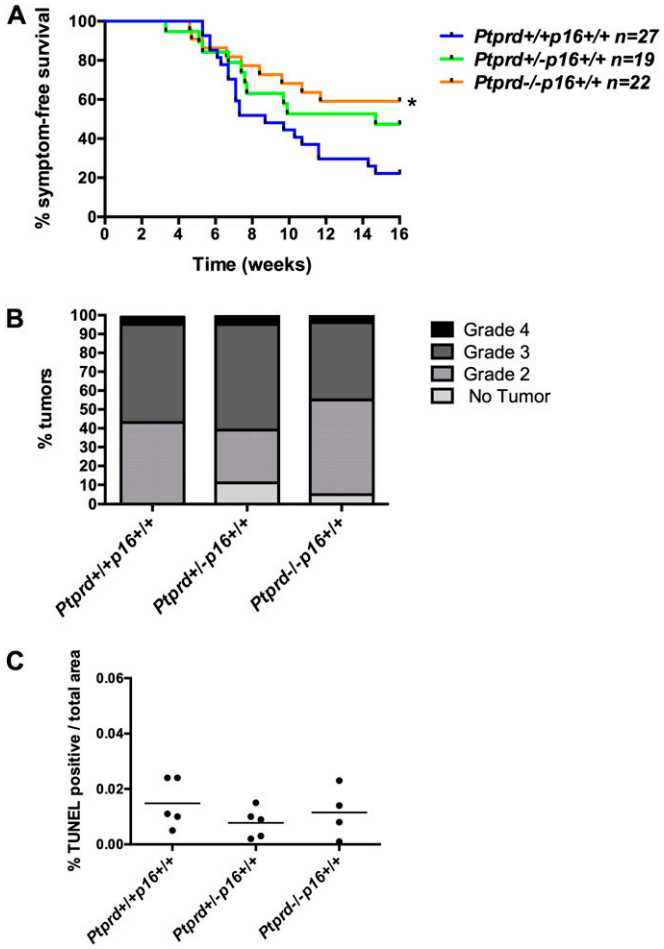

Fig. S2. Mice with *Ptprd* loss require deletion of *Cdkn2a/p16*^{Ink4a} for tumorigenesis. (*A*) Kaplan–Meier survival curve of mice infected with RCAS-PDGFB and followed for 16 wk. *Ptprd*$^{+/+}$*p16*$^{+/+}$ ($n = 27$), *Ptprd*$^{+/-}$*p16*$^{+/+}$ ($n = 19$), *and Ptprd*$^{-/-}$*p16*$^{+/+}$ ($n = 22$). **Ptprd*$^{-/-}$*p16*$^{+/+}$ vs. *Ptprd*$^{+/+}$*p16*$^{+/+}$ $P < 0.05$. (*B*) Tumors graded according to World Health Organization standards. (*C*) Metamorph quantification of TUNEL staining on *Ptprd*$^{+/+}$*p16*$^{+/+}$ ($n = 5$), *Ptprd*$^{+/-}$*p16*$^{+/+}$ ($n = 5$) *and Ptprd*$^{-/-}$*p16*$^{+/+}$ ($n = 4$) tumors. No significant differences in cell death were observed.

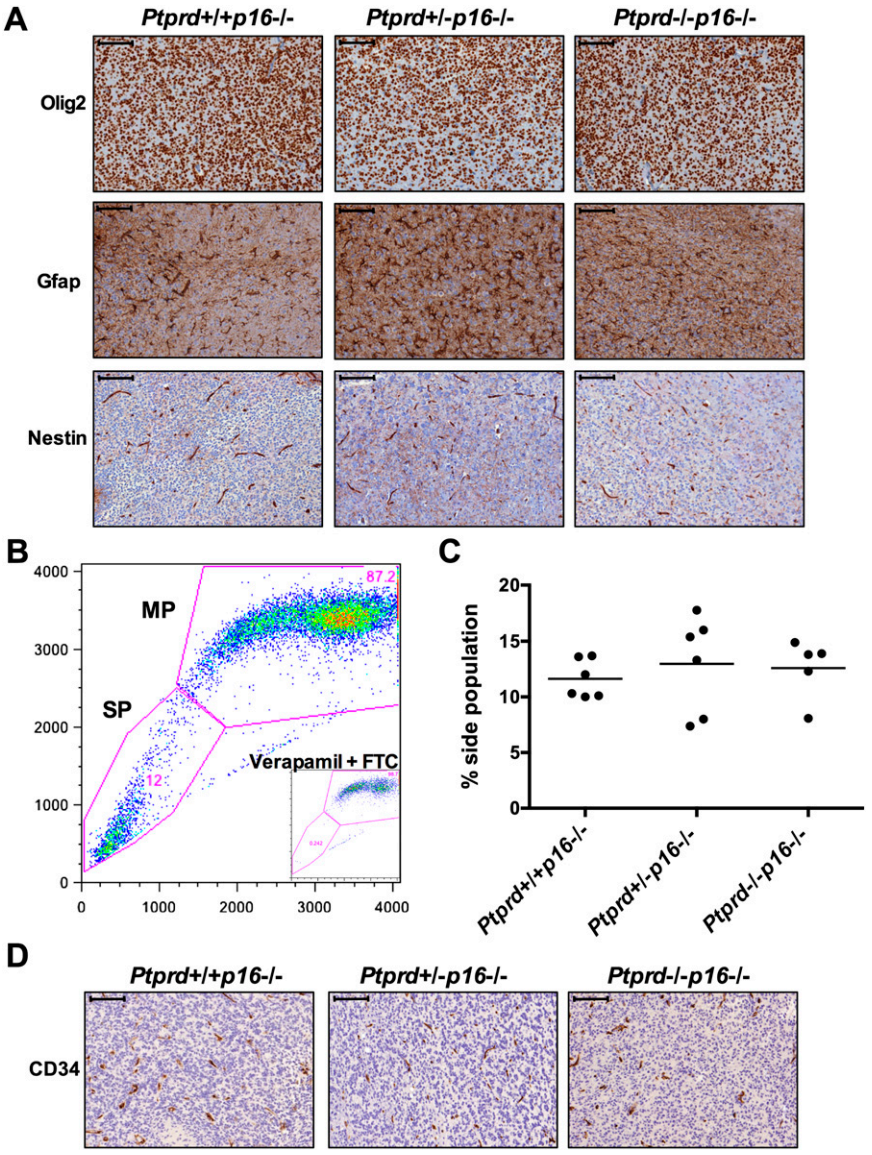

Fig. S3. *Ptprd* loss does not affect differentiation, the glial stem cell pool, or angiogenesis. (*A*) Representative images of immunohistochemistry performed on RCAS-PDGFB tumors for Olig2 (oligodendrocytes), Gfap (astrocytes), and Nestin (glial progenitors). (Scale bars, 100 μm.) (*B*) Representative image of side population analysis (Hoechst 33422 dye exclusion) that was performed on RCAS PDGFB-GFP tumors. (*Inset* graph) Verapamil and fumitremorgin c (FTC) ABCG2 transporter inhibitors were applied to the samples tested to set population gates. MP, main population; SP, side population. (*C*) Quantification of side population analysis. No differences in the glial stem cell pool were observed. (*D*) Representative images of CD34 immunohistochemistry performed on RCAS PDGFB stereotactically injected tumors. No differences in vascular density were observed. (Scale bars, 100 μm.)

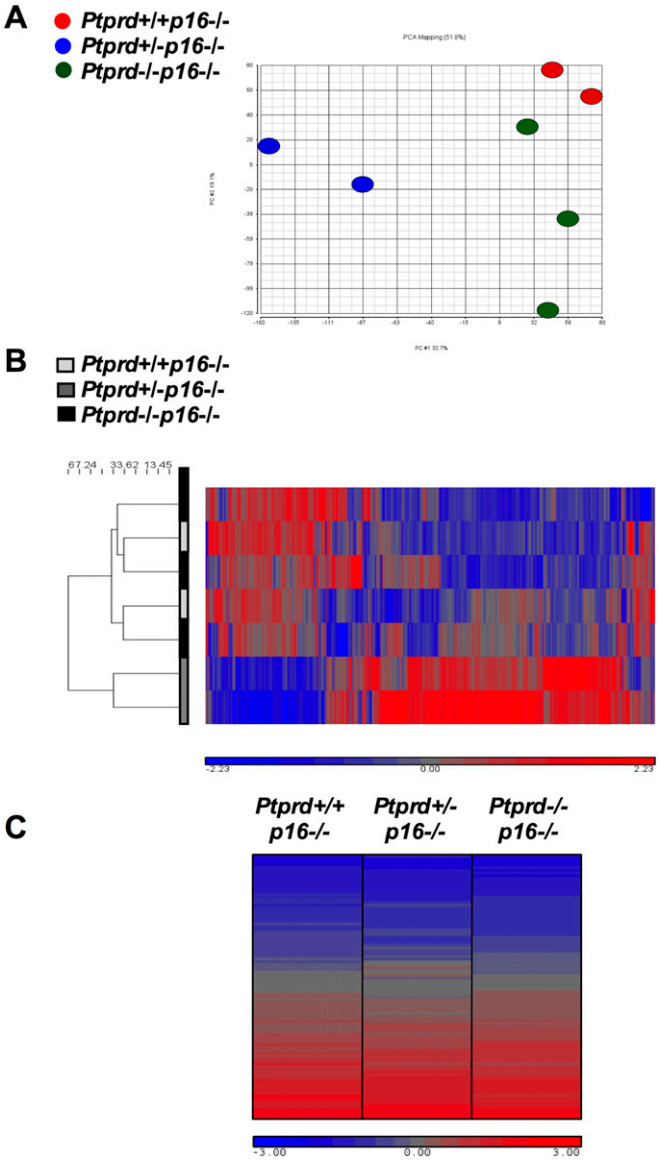

Fig. S4. Heterozygous *Ptprd* loss leads to distinct gene-expression changes. (*A*) Principal component analysis of expression microarray data from tumors of each genotype. Duplicates represent biological replicates. (*B*) Hierarchical clustering of expression microarray data from each genotype. Color bar depicts normalized gene expression levels. (*C*) Heat map of tyrosine phosphatase gene expression from microarray data. Color bar depicts normalized gene expression levels. Average expression of each genotype is shown.

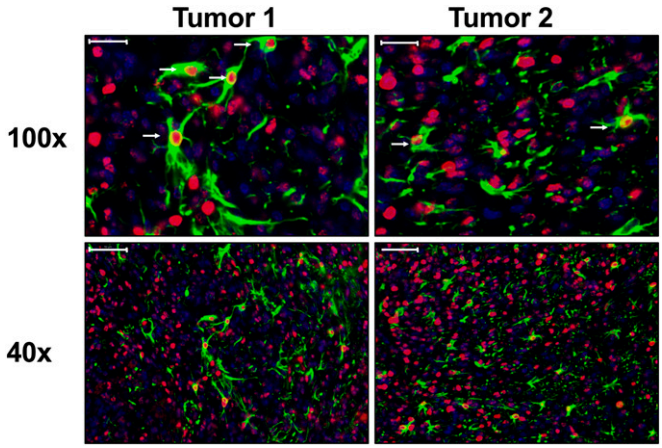

Fig. S5. Glial cells within *Ptprd*$^{+/-}$*p16*$^{-/-}$ tumors express p-Stat3. Coimmunfluorescence of Gfap and p-Stat3 was performed on *Ptprd*$^{+/-}$*p16*$^{-/-}$ tumors. White arrows point to cells with cytoplasmic Gfap and nuclear p-Stat3. Representative images from two tumors are shown. [Scale bars, 20 μm (*Upper*) and 50 μm (*Lower*).]

Table S1. Concordance of *PTPRD* loss with other common gene alterations in GBM

Gene	Altered in samples with *PTPRD* loss			Altered in samples with diploid *PTPRD*			Ratio	*P* value
PDGFRA	6	55	11%	8	80	10%	1.10	2.20E-01
NF1	9	55	16%	12	80	15%	1.07	1.85E-01
PTEN	14	55	26%	31	80	39%	0.67	4.11E-02
PIK3CA	5	55	9%	5	80	6%	1.50	2.12E-01
PIK3R1	6	55	11%	6	80	8%	1.38	1.88E-01
CDKN2A	**41**	**55**	**75%**	**21**	**80**	**26%**	**2.88**	**2.30E-08**
CDKN2B	**44**	**55**	**80%**	**26**	**80**	**33%**	**2.42**	**3.38E-08**
CDKN2C	1	55	2%	3	80	4%	0.50	3.41E-01
TP53	13	55	24%	30	80	38%	0.63	3.60E-02
MDM2	5	55	9%	11	80	14%	0.64	1.58E-01
MDM4	1	55	2%	6	80	8%	0.25	1.19E-01
RB1	2	55	4%	12	80	15%	0.27	2.35E-02
CDK4	5	55	9%	17	80	21%	0.41	3.29E-02
CDK6	1	55	2%	1	80	1%	2.00	4.86E-01

PTPRD loss includes homozygous and heterozygous events. Boldface indicates that CDKN2A/CDKN2B are significantly co-occuring with PTPRD loss.

Table S2. *PTPRD* loss within GBM transcriptional subtypes

Subtype	Loss	Total loss	Percent loss (%)
Classical	18	54	33
Neural	14	54	26
Proneural	11	54	20
Mesenchymal	11	54	20

Homozygous and heterozygous events are included.

Table S3. Stat3 gene targets

Gene ID	Fold-change
Timp1	15.27
Gadd45g	7.72
Gbp2	7.46
A2m	6.35
Bcl3	6.20
Vim	5.84
Cdkn1a	5.78
Gfap	5.04
Hk2	4.49
Col3a1	4.39
Cebpd	3.57
Gja1	3.41
Socs3	3.22
Myc	2.93
Tap1	2.75
Col1a2	2.57
Zfp36	2.54
Vegfa	2.05
Ccne1	2.03
Junb	2.01
Ptpn2	1.86
Ppargc1a	−3.38

Stat3 gene targets altered in $Ptprd^{+/-}p16^{-/-}$ tumor cells. Average fold-change over $Ptprd^{+/+}p16^{-/-}$ tumors.

Table S4. Tyrosine phosphatase gene-expression

Gene symbol	*Ptprd*$^{+/+}$*p16*$^{-/-}$	*Ptprd*$^{+/-}$*p16*$^{-/-}$	*Ptprd*$^{-/-}$*p16*$^{-/-}$
Dusp1	8.98	9.35	9.25
Dusp10	3.60	3.61	3.54
Dusp10	5.97	6.86	6.42
Dusp11	8.63	8.43	8.52
Dusp11	9.31	9.04	9.15
Dusp12	7.24	6.72	7.17
Dusp12	4.77	4.78	4.97
Dusp14	6.24	7.11	6.44
Dusp15	7.65	6.85	7.68
Dusp16	8.32	7.68	8.49
Dusp18	6.82	7.08	6.67
Dusp19	7.78	8.07	8.15
Dusp19	6.90	6.73	7.11
Dusp2	5.03	5.06	5.01
Dusp22	7.16	6.98	7.31
Dusp26	9.51	9.22	9.32
Dusp3	5.87	5.57	5.60
Dusp3	8.46	8.46	8.46
Dusp6	11.13	10.50	11.27
Dusp7	7.73	7.30	7.67
Dusp7	7.39	6.97	7.27
Dusp7	5.35	5.22	5.34
Dusp8	7.09	6.47	7.01
Dusp9	4.03	4.11	4.20
Dusp9	3.69	3.74	3.46
Dusp9	3.40	3.49	3.44
Eya1	5.51	4.75	5.44
Pten	9.16	9.16	9.07
Pten	9.24	8.96	8.96
Pten	10.20	9.97	10.11
Ptpn1	8.62	8.89	8.78
Ptpn1	7.76	7.88	7.82
Ptpn11	4.26	4.30	4.13
Ptpn11	7.27	7.69	7.28
Ptpn11	9.62	9.62	9.43
Ptpn12	10.88	10.59	10.73
Ptpn12	8.10	7.82	7.76
Ptpn12	9.10	8.94	8.85
Ptpn12	10.16	9.89	9.95
Ptpn13	3.58	3.42	3.63
Ptpn13	5.59	6.55	6.32
Ptpn14	4.87	4.87	4.85
Ptpn14	4.42	4.34	4.21
Ptpn18	4.98	5.34	5.09
Ptpn2	8.46	8.90	8.49
Ptpn2	5.19	5.38	5.03
Ptpn2	3.05	3.64	3.28
Ptpn2	8.61	8.84	8.67
Ptpn20	5.29	5.11	5.50
Ptpn21	6.89	6.42	6.85
Ptpn21	6.73	6.54	6.86
Ptpn21	5.47	4.86	5.24
Ptpn22	3.22	3.36	3.41
Ptpn23	6.86	6.69	6.86
Ptpn4	5.20	4.85	4.87
Ptpn5	7.41	7.05	7.44
Ptpn5	4.48	4.21	4.55
Ptpn5	5.81	5.76	5.95
Ptpn6	5.88	6.09	6.10
Ptpn6	3.63	4.06	3.67
Ptpn9	8.51	8.23	8.49
Ptpra	9.81	9.41	9.84
Ptprb	5.24	5.50	4.74

Table S4. Cont.

Gene symbol	*Ptprd*$^{+/+}$*p16*$^{-/-}$	*Ptprd*$^{+/-}$*p16*$^{-/-}$	*Ptprd*$^{-/-}$*p16*$^{-/-}$
Ptprc	4.08	5.50	4.41
Ptprd	10.68	9.27	9.23
Ptprd	10.83	9.24	9.58
Ptprd	9.64	8.05	8.27
Ptpre	10.19	9.73	9.91
Ptpre	10.56	10.00	10.38
Ptprf	6.72	6.70	6.50
Ptprf	9.43	9.44	9.36
Ptprf	9.47	9.29	9.30
Ptprg	8.18	7.79	8.04
Ptprj	3.34	3.14	3.28
Ptprj	4.16	3.94	4.04
Ptprj	3.97	3.71	3.90
Ptprj	7.50	6.99	7.31
Ptprk	7.29	7.04	7.27
Ptprk	8.61	7.84	8.53
Ptprk	5.14	4.86	4.62
Ptprm	7.76	7.00	7.67
Ptprn	7.43	7.83	7.79
Ptprn2	4.31	4.20	4.39
Ptpro	9.79	9.17	9.72
Ptpro	6.43	5.75	6.04
Ptprr	7.64	6.44	7.46
Ptprs	11.07	10.69	11.05
Ptprs	3.74	3.73	3.91
Ptprs	5.09	4.48	4.96
Ptprt	4.92	4.80	4.84
Ptprt	8.24	7.56	7.81
Ptpru	7.89	7.26	7.82
Ptprv	4.45	4.92	5.04
Rngtt	6.41	6.64	6.43
Rngtt	6.90	6.61	6.76
Styx	3.55	3.65	3.47
Tenc1	5.50	5.97	5.24
Tpte	4.48	4.49	4.51

Tyrosine phosphatase gene-expression within *Ptprd*$^{+/+}$*p16*$^{-/-}$, *Ptprd*$^{+/-}$*p16*$^{-/-}$, and *Ptprd*$^{-/-}$*p16*$^{-/-}$ tumors. An average of normalized gene-expression values for each genotype are shown.

Table S5. Ingenuity Pathway Analysis of *Ptprd*$^{+/-}$*p16*$^{-/-}$ tumors

Category	Predicted activation state	*P* value	Bias corrected *z*-score	No. of molecules
Immune cell trafficking				
Migration of macrophages	Increased	4.59E-05	2.8	13
Migration of antigen presenting cells	Increased	8.61E-05	2.8	19
Migration of phagocytes	Increased	3.60E-05	2.5	27
Cell movement of myeloid cells	Increased	1.59E-05	2.0	44
Inflammatory response				
Migration of macrophages	Increased	4.59E-05	2.8	13
Migration of phagocytes	Increased	3.60E-05	2.5	27
Phagocytosis	Increased	2.11E-05	2.5	28
Phagocytosis of cells	Increased	2.70E-05	2.2	26
Immune response of cells	Increased	1.05E-04	2.2	29
Phagocytosis of tumor cell lines	Increased	3.55E-04	2.0	10
Cell movement				
Migration of macrophages	Increased	4.59E-05	2.8	13
Migration of antigen presenting cells	Increased	8.61E-05	2.8	19
Migration of phagocytes	Increased	3.60E-05	2.5	27
Migration of cells	Increased	8.86E-19	2.3	155
Cell movement	Increased	5.32E-20	2.1	170
Migration of blood cells	Increased	3.89E-09	2.1	75
Invasion of tumor cell lines	Increased	2.06E-15	2.0	68
Cell movement of myeloid cells	Increased	1.59E-05	2.0	44